Fast switchable field-induced optical birefringence in highly transparent polymer-liquid crystal composite

YOUNG JIN LIM,[1,4] **JEONG HWAN YOON,**[2,4] **HYESUN YOO,**[1] **SEONG MIN SONG,**[1] **RAMESH MANDA,**[1] **SRINIVAS PAGIDI,**[1] **MYONG-HOON LEE,**[3] **JAE-MIN MYOUNG,**[2,5] **AND SEUNG HEE LEE**[1,*]

[1]*Applied Materials Institute for BIN Convergence, Department of BIN Convergence Technology and Department of Polymer Nano Science and Technology, Chonbuk National University, Jeonju, Jeonbuk, 54896, South Korea*
[2]*Department of Materials Science and Engineering, Yonsei University, Seoul 03722, South Korea*
[3]*Graduated School of Flexible and Printable Electronics, Chonbuk National University, Jeonju, Jeonbuk, 54896, South Korea*
[4]*Both authors contribute equally*
[5]*jmmyoung@yonsei.ac.kr*
[*]*lsh1@chonbuk.ac.kr*

Abstract: A liquid crystal device with optically isotropic liquid crystal (OILC) phase induced from polymerization-induced phase separation exhibit a fast response time and a proper dark state. Its electro-optic performances are highly influenced by a kind of materials and processing conditions. Here, the effect of materials and phase-separation on the electro-optic performance of OILC device has been investigated by utilizing the acrylate and the thiol-ene monomer mixtures. The optically isotropic phase was analyzed with scattering theory, and it was revealed that a novel polymer network structure of acrylate mixture is free of scattering and yields a higher on-state transmittance, enhanced by ~50%. By tuning the monomer ratio and UV intensity, an excellent transparent film was obtained and, in addition, the response time was improved by ~40%. The excellent black state and its flexibility can be applied to flexible liquid crystal photonic and display devices.

1. Introduction

The optically isotropic liquid crystal (OILC) mixture is newly emerging in liquid crystal displays (LCDs) because the composite is transparent in the visible light and its electro-optic performances can be kept even it is either curved or bent because LC droplets are embedded in the polymer matrix [1–3]. The OILC exhibits an optically isotropic phase originated from nano-structured LC in a polymer matrix and becomes an optically anisotropic with induced birefringence on electric field application. Applying it to LCD technology, the OILC offers an advantage of wider viewing angle and sub-millisecond response time which can applicable to full-color field-sequential display. It is also a potential candidate to flexible display due to confined nano-sized LC droplets in a polymer matrix and no fixed predetermined macroscopic LC orientation [4]. However, the crucial problem that exists in this type is the light leakage which depends on the existence of few bigger droplets larger than wavelength of incident light. To overcome this problem many approaches have been explored in detail and their electro-optical properties are greatly improved [3–6]. Additionally, the hysteresis free and high contrast ratio OILC device has been reported by utilizing novel polymer architectures [7]. However, the electro-optic properties of OILCs are not only influenced by droplet size but also micro-structure of the polymer network.

Usually, the Rayleigh-Gans scattering theory explains the scattering from a film having smaller particles compared to the incident radiation. Implementing the Rayleigh-Gans

scattering theory to this nano-structured LC, the scattering cross-section can be expressed as [8,9],

$$\sigma_{avg} \propto |m-1|^2 \, \Gamma^4 D^6, \tag{1}$$

where Γ ($= 2\pi n_p/\lambda$) is the magnitude of the wave vector, λ is the wavelength of the radiation, n_p is the refractive index of the polymer matrix, D is the diameter of LC domain in a polymer matrix, and m is refractive index ratio between LC and polymer (n_{LC}/n_p). To obtain a scattering free film, the LC droplets must be smaller than the wavelength of incident light ($D < \lambda$) and, in addition, the effective refractive index of LC droplet (n_{LC}) should match with refractive index of the polymer network (n_p). When a strong electric field is applied to this phase, the induced birefringence (Δn_{ind}) occurs parallel to the applied field (E) when using a LC with positive dielectric anisotropy (Δe), known as Kerr effect, following the relationship $\Delta n_{ind} = K\lambda E^2$, where K is Kerr constant proportional to magnitude of Δn and Δe of a LC [10–12]. The Kerr effect has extensively been studied in nano-structured LC based OILCs. A few bigger droplets generated during phase-separation causes a slight light leakage which could severely affect a dark state and transmittance of an OILC device. On the other hand, if D is too small with respect to incident radiation, a higher driving voltage is required to have Δn_{ind}, which makes it difficult to use conventional LCD drivers. Therefore, optimizing the droplet size and physical properties of LC is a key parameter to improve the device performance. Furthermore, the D is decided by the concentration ratio of LCs and monomer, while the architecture of the polymer network is manipulated by controlling the steps in phase-separation process and type of monomers used [3]. In addition, many variable parameters such as UV intensity and time also contributes to form OILC phase, which increases the complexity in choosing the right materials and precisely controlling the phase separation.

In our previous work, the maximum LC concentration to achieve an efficient isotropic phase was limited to 42 wt% relative to the monomer NOA65, which is quite low to induce the high Kerr constant. Even though the higher LC concentrations were reported, a severe light scattering was noticed which turns OILC to be pseudo-OILC [12,20]. Therefore, it is always desirable to make an OILC with smaller LC droplets and with coexistence of high filling factor of LC which can exhibit higher Kerr constant without sacrificing efficiency of the isotropic property [13–15]. In order to achieve this kind of device, a novel polymer structures need to be explored. Also, the polymer network formation mechanism and associates electro-optics are need to be investigated in detail.

In this report, we attempt to develop a scattering free OILC film based on a polymerization induced phase-separation (PIPS) method by tuning the UV intensity and monomer concentration [16,17]. We utilized two different monomers NOA65 and PN393 comprised of thiol-ene and acrylate functional groups, respectively, and systematically examined the influence of phase-separation and material concentrations on electro-optic characteristics of the OILC device. The OILC phase was analyzed with scattering theory in detail. Interestingly, the OILC film with PN393 exhibits the higher transparency which gives rise to an excellent dark state and, in addition, higher on-state transmittance was achieved.

2. Experiments

The prepared OILC composites consist of high dielectric constant nematic LC mixture, MLC-2053 (T_{NI} = 86 °C, $\Delta\varepsilon$ = 46.2, n_e = 1.7472, n_o = 1.5122, Δn = 0.235 at 589.3 nm, 20 °C, from Merck Advanced Technology in Korea) and the UV curable monomers. The mixture was injected into the in-plane switching (IPS) cell by capillary action at 88 °C. The IPS cell consists of ITO deposited interdigitated electrodes on bottom substrates while no electrode exists on top substrate. Both electrode width and spacing between them were 4 μm and the cell gap was fixed to 10 μm. The cells were irradiated with UV light (365 nm peak) to initiate

the phase-separation at room temperature. We have utilized two types of monomers: one is a Norland Optical Adhesive 65 (NOA65, n_p = 1.5275 at 589 nm, from Norland Products Inc.) and the other is a monomer mixture PN393 (n_p = 1.473 at 589 nm, from Merck Advanced Technology in Korea). The NOA65 is a thiol-ene based optical adhesive, particularly, it is a mixture of 42 wt% of trimethylolpropanetris thiol, 3 wt% of trimethylopropane diallyl ether, 54 wt% of isophorone diisocyanate ester, and 1 wt% of benzophenone as the photo-initiator. The PN393 is mixture of few acrylate monomers comprised of different acrylates such as 87 wt% of acrylic acid 2-ethylhexyl ester (EHA), 2 wt% of trimethylolpropane triacrylate (TMPTA), 1 wt% of diphenyl (2, 4, 6-trimethylbenzoyl) phosphine oxide and 2-Hydroxy-2-methylpropiophenone (Darocur4265), and 10 wt% of Ebercyl1810. The long alkyl chains in acrylate monomers in PN393 are believed to provide more flexibility to the structure. All these materials were used without further purification.

The polarized optical microscope (POM), Nikon ECLIPSE E600 (Nikon, Japan) equipped with Nikon DXM 1200 digital camera, was used to characterize optically isotropic phase under crossed polarizers. The electro-optical properties were measured as a function of voltage by using a lab made set-up under crossed polarizers. The electric field was applied to the sample by using a function generator (Agilent 33521A) and transmitted light was detected by photo-detector and oscilloscope (Tektronix DPO 2024B). Finally, the LC was extracted from the cell and the polymer network morphology was characterized by using field emission scanning electron microscope (FESEM).

3. Results and discussion

The schematic of switching principle of OILC device in an IPS cell under crossed polarizers has shown in Fig. 1. As we understood from Eq. (1), if D is smaller than 350 nm and the effective n_{LC} is matched to n_p, the scattering (σ_{avg}) of the film becomes zero. Therefore, the phase exhibit an optically isotropic state in the visible light region. The transmittance of the light passing through this phase under crossed polarizers can be expressed as,

$$T_{LC} = T_o \sin^2 \left(2\psi(V) \right) \sin^2 \left(\frac{\pi d \Delta n_{ind}(V)}{\lambda} \right), \tag{2}$$

where T_{LC} is a transmittance factor from the retardation ($d\Delta n_{ind}(V)$) due to LC reorientation responding to applied voltage, ψ is the angle between the polarizer and field induced LC director, and d is cell gap. At isotropic phase (V = 0), the $d\Delta n_{ind}$ is zero for any angle of ψ. Therefore, the incident polarized light is not affected by the phase and consequently stopped by the analyzer, showing a dark state as shown in Fig. 1(a). When an electric field is applied, the induced birefringence (Δn_{ind}) becomes non-zero with ψ = 45°, then the device shows a a bright state, as shown in Fig. 1(b) [10–12,18,19]. In order to maximize transmittance, $d\Delta n_{ind}$ should be $\lambda/2$. However, the field induced birefringence is not uniform all over the phase such that the transmittance depends on horizontal position.
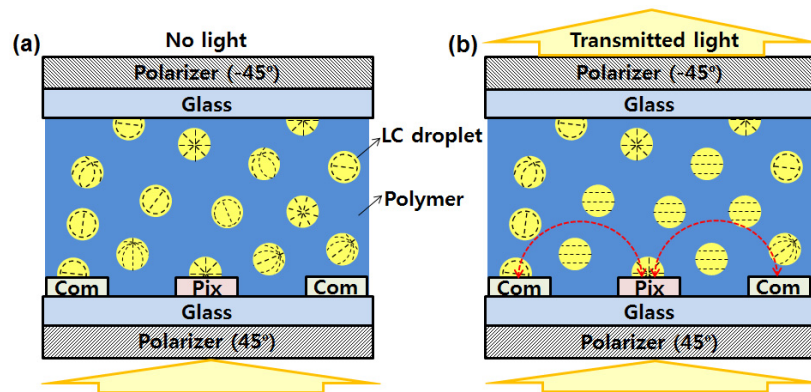
Fig. 1. The schematic of OILC driving mechanism under in-plane filed at, (a) voltage-off dark state (optically isotropic state) and (b) voltage-on bright state (optically anisotropic state).

It is well known that the concentration of the monomer plays an important role on droplet formation. Therefore, in a first step, it is important to understand the monomer concentration effect on droplet size. Therefore, we have prepared three different mixtures using MLC-2053 and PN393 with varying weight percent 40:60, 45:55, and 50:50 wt.% and then phase separation was performed by irradiating 80 mW/cm^2 intensity of UV light for 10 s at room temperature. The resulted phase was analyzed with using POM, and voltage-dependent transmittance (V-T) characteristics were measured as illustrated in Fig. 2. Under POM, three cells showed a good dark state and it was unaltered while rotating the sample under crossed polarizers, which is a clear indication of optically isotropic phase. The efficiency of dark state was estimated by using i-solution image analyzer software (iMT, i-Solution Inc., Canada). Calculated relative light leakages are 5.5, 5.5, and 5.6 for 60, 55, and 50 wt.% of PN393, respectively. The V-T curves show an induced birefringence starts to generate with increasing the applied voltage and then get saturated at high enough voltage. The threshold voltage (V_{th}) and operating voltage (V_{op}) are defined as the voltage required for the transmittance to reach 10% and 90% of the saturation transmittance, respectively. The measured V_{op} were approximately 38.5, 32.1, and 29.3 V and the relative on-state transmittance were 2.6, 5.5, and 7.6% for 60, 55, and 50% of PN393 concentration, respectively. The highest on-state transmittance of 50% PN393 sample indicates that the higher LC amount, the more birefringence is induced. The V_{op} is reduced with decrease of PN393, in contrast, whereas the V_{th} is showing mixed trend. In addition, we achieved an excellent dark state even though the concentration of LC is much higher for 50:50 wt.% sample compared to conventional OILCs with NOA65, which turns to be a dramatic improvement on electro-optical properties. Overall, the electro-optic properties were greatly improved for 50% PN393 concentration as confirmed by increased in on-state transmittance. This trend is in good agreement with previous studies [7,20]. Therefore, we fix the PN393 concentration to 50 wt.% and studied phase-separation effect on electro-optic properties.
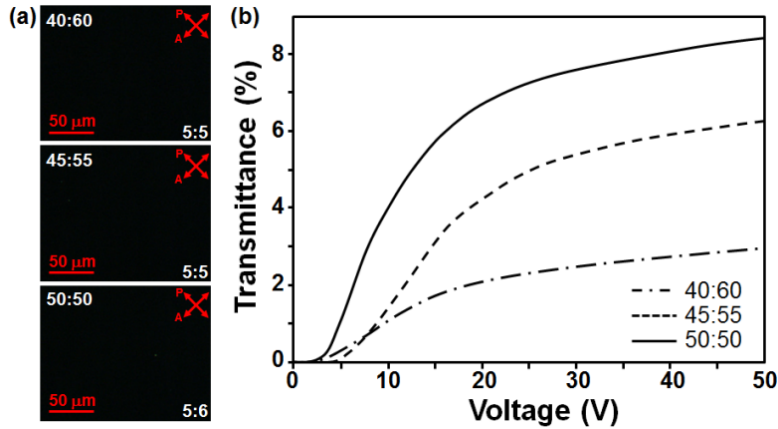
Fig. 2. (a) POM images at 0 V, and (b) Voltage-dependent transmittance curves of OILC cells at three different material concentrations which correspond to MLC 2053:PN393 = 40:60 wt.%, 45:55 wt.%, and 50:50 wt.%, respectively.

In a second step, we attempted to optimize the phase-separation by tuning the UV intensity and time duration when the concentration of PN393 is 50:50 wt.%. After phase separation with different UV intensities, electro-optic characteristics of all cells were examined and compared with NOA65 [20–22]. Table 1 shows a list of prepared OILC mixtures and phase-separation conditions. Small amount of photo-initiator, Irgacure651 (2, 2-Dimethoxy-1, 2-diphenylethan-1-one), was added to the S1, while remaining samples consist of pre-dissolved photo-initiator, Darocur4265.

Table 1. Concentration ratio of LC and monomer and irradiated UV intensity for all OILC cells in the experiments.

Cell label	Concentration ratio	UV intensity
S1	MLC 2053: NOA65 = 40:60 wt.%	150 mW/cm^2 for 5 s
S2	MLC 2053: PN393 = 50:50 wt.%	60 mW/cm^2 for 12 s
S3	MLC 2053: PN393 = 50:50 wt.%	70 mW/cm^2 for 10 s
S4	MLC 2053: PN393 = 50:50 wt.%	80 mW/cm^2 for 10 s

The POM images were taken under crossed polarizers while keeping the intensity of light source unchanged all over the experiment. The obtained results are shown in Fig. 3(a). The measured intensity of the dark state were 18, 6.5, 5.8, and 5.6 for S1, S2, S3 and S4, respectively, which reveals the obtained PN393 samples are relatively free of scattering although the amount of LC is much higher than that of S1. Even though, the n_p of NOA65 is much closer to n_{eff} of LC, the PN393 is showing less scattering. Figure 3(b) shows macroscopic scattering images of bulk cells which also reveals the same, as the text under the cell is clearly appearing for PN393 samples while small scattering is noticed for NOA65 sample. However, the sample S4, which is cured at high intensity and longer time duration, exhibits a less scattering, indicating an excellent optically isotropic phase.
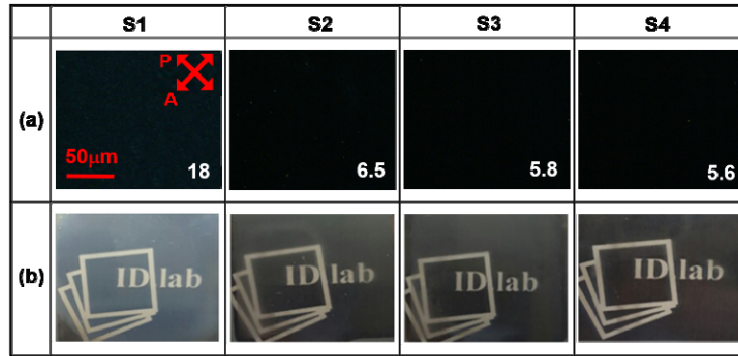
Fig. 3. (a) Off-state POM images under crossed polarizers. Represented numbers inside the dark images indicate light leakage), and (b) Macroscopic images without crossed polarizers of all OILC cells. The cell was placed 5 cm above the "ID lab" phrase written on a dark paper.

In order to find out a detailed reason for light leakage, the wavelength dependent transmittances was examined before and after LC extraction using an UV-Visible spectroscopy. The obtained transmission spectra in the visible wavelength region have been shown in Fig. 4. Corresponding photographic images of bulk cells have been taken in both cases, shown as insert image. Here, the LC was extracted from the cell by dissolving into hexane-dichloromethane (ratio: 80:20 wt.%) solvent for one day [23]. The wavelength dependent measurements were performed without polarizers at voltage-off state. Interestingly, the wavelength dependent transmission of the S1 is increased, from 70% to 87%, after LC extracted. In contrary, the transmission of the sample S4 is decreased, from 84% to 76%, after LC extraction. It is obvious that, after LC extraction, the scattering would be due to the refractive index mismatches between n_p and air ($n = 1$) which could fill the pore after LC washed out. Assuming that the pores/voids in S1 and S4 are empty, one could easily infer that some amount of LC is remained inside the polymer networks in S4 even after LC extraction. According to Eq. (1), the σ_{avg} is also influenced by the refractive index ratio m (= n_{LC}/n_p), that is, if the m is closer to 1, the scattering minimizes. The experimental results indicate that the n_p of PN393 is expected to increase after phase-separation.
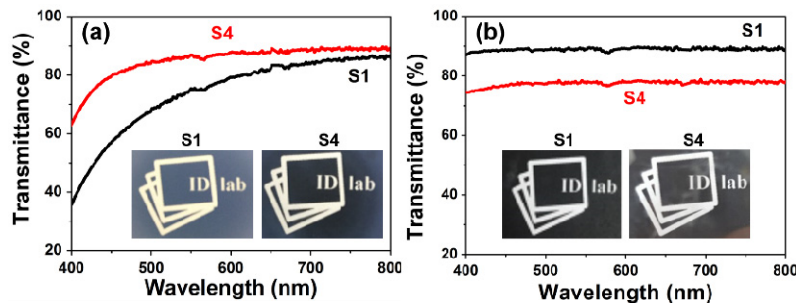

Fig. 4. The UV visible wavelength-dependent transmittance curves of S1 and S4 (a) before and (b) after removing LC. Corresponding photographic images were shown as inset.

Now, how n_p of PN393 could be changed after phase-separation is speculated when assuming some amount of LC remained in the polymerized network. Here, the effective refractive index of polymer network (n_p') and refractive index ratio (m) are estimated by using an empirical equation after LC extraction [24]. In LC and polymer mixtures, the refractive index of porous type materials depends relay on volume fraction of the pores and as well as materials occupied inside the pores. The effective refractive index (n_p') of the polymer network of PN393 with filled LC in the pore is given by,

$$n_p^{'} = n_{LC}\upsilon_{LC} + n_p\upsilon_p,\qquad\qquad(3)$$

where n_{LC} is the average refractive index ($= (n_e + 2n_o)/3$) of LC material and n_p is refractive index of polymer network. Here, υ_{LC} and υ_p stand for the volume fraction of LC and polymer network, respectively. The results calculated from Eq. (3) suggest 47% of LC remains in polymer network, so that m should be less than 1.0413 for S4, as shown in Fig. 5. The estimated value is rather high, but it explains the increased scattering in the polymer network of PN393 after LC is extracted. When υ_{LC} is zero, i.e., LC is completely extracted, the m is largely deviate from unity. Similarly, when υ_{LC} = 0.5, the m reaches closer to the unity at which the scattering cross section (σ_{avg}) become zero.
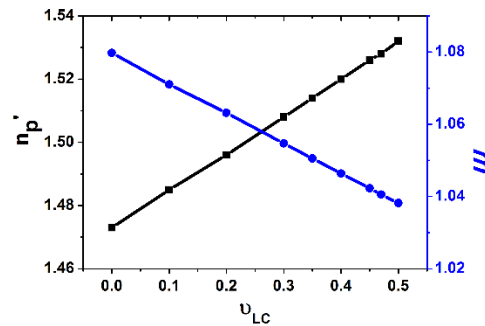

Fig. 5. The modified values of n_p' and m as a function of υ_{LC}.

The polymer network morphology was studied by using the FESEM and the calculated statistic histogram of the size distribution was shown in Fig. 6. The average droplet size was calculated by fitting with a Gaussian function (blue line). The calculated average droplet size is 206, 211, 203, and 199 nm for the S1, S2, S3, and S4, respectively. The results confirm that the LC droplets in all the samples are much smaller than that of the incident wavelength. However, slight difference in the polymer architecture was noticed between thiol-ene monomer sample (S1) and acrylate monomers samples (S2, S3, and S4). The close observation of polymer structure suggests that the discrete and uniformly shaped droplets separated by a very thin polymer layer were obtained in sample S2 and S3. The irregular and uneven surfaces with isolated droplets were achieved for sample S1 while relatively coarse surfaces with droplets were found for sample S4 which was cured at highest intensity. Quite number of larger droplets over 200 nm for PN393 can be noticed in S2 and S3 such that the number of droplets over 200 nm follows the order, S4<S3<S2, which also explains why the scattering decreases in order of S2, S3 and S4. In addition, the calculated filling factors of droplets over whole measured area for PN393 are 48, 47, and 40% for samples S2, S3, and S4, respectively. The variations of filling factors would be associated with degree of dissolutions of LC in a polymer matrix, i.e. the more LC is dissolved in a polymer network, and the fill factor becomes less.
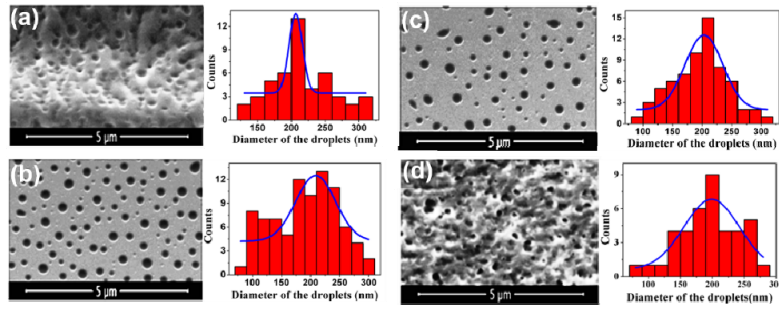
Fig. 6. Obtained polymer micro-structures and histogram of droplet sizes distribution of all OILC cells, (a) S1, (b) S2, (c) S3, and (d) S4.

We also measured electro-optic properties for all the samples. He-Ne laser (λ = 633 nm) light was probed under crossed polarizers condition and the transmitted light intensity was measured with Eq. (2). The sample with IPS electrodes was driven by 1 kHz square wave field and voltage-dependent transmittances are illustrated in Fig. 7(a). The measured V_{th} are 4.0, 5.0, 4.7, and 4.5 V, and relative maximum on-state transmittances are 11.4, 17.2, 14.1, and 8.4% for the S1, S2, S3, and S4, respectively. The field induced birefringence tends to saturate at higher enough field. Interestingly, the on-state transmittance was significantly higher for S2 than other cells though V_{th} is slightly higher among the cells with PN393. Droplet size and distribution from FESEM images could explain the electro-optic results such that the highest fill factor of the droplets in S2 gives highest induced birefringence, resulting in highest transmittance and the total number of droplets whose size is smaller as well as larger than 200 nm is largest in S2, which may explain a slight high V_{th} compared to others due to smaller droplets. The relatively less amount of LC in a polymer network in S2 compared to S4 could explain higher fill factor of LC droplets. From above results, one can easily confirm that the fill factor of LC droplets is a major factor determining the field-induced birefringence and keeping LC droplet size not too small less than 150 nm is also important for reduction of a V_{th}.

The response time was measured as the LC response to the 1 kHz square wave field. Here, the rising time (decaying time) corresponds to 80% transmittance chance from 10% (90%) to 90% (10%). From Fig. 7(b), the measured rising times were 600, 476, 384, and 395 µs and decaying times were 4.4, 2.7, 1.7, and 1.9 ms, for S1, S2, S3 and S4, respectively. Even though we have utilized a high dielectric anisotropy NLC, we achieved a fast response time. The rising time is governed by the magnitude of applied field. On other hand, the decaying time is defined as the director relaxation which is strongly influenced by LC interaction at polymer walls and visco-elastic coefficient of LC. However, in this case, we speculate that the variation in decaying time would be attributed from delicate interplay between the droplet size and LC anchoring energy. The decaying time for OILC is expressed as [25],

$$\tau_d \approx \frac{\gamma_1 D^2}{k_{eff} W_s (2\pi)^2},\qquad(4)$$

where γ_1 is the rotational viscosity of the LC, k_{eff} is the effective elastic constant of LC, W_s is the LC anchoring energy at polymer walls, and D is the size of the LC droplet. From the above equation, Eq. (4), it is clear that the decaying time is proportional to D^2. Therefore, the fast decaying time for sample S3 and S4 compared to S2 is attributed to smaller average LC droplets. Even though, the sample S2 is exhibiting higher on-state transmittance, the slightly slow response time would be a demerit to this sample. Therefore, it is required to optimize materials and phase-separation more precisely to improve the electro-optic properties of OILC.
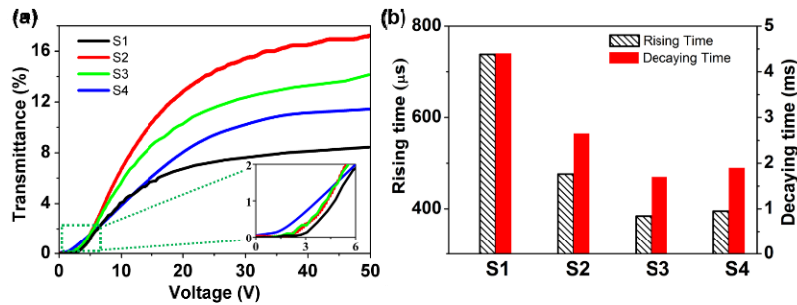
Fig. 7. Measured (a) voltage-transmittance curves and, (b) response time of prepared OILCs at different UV intensity.

4. Conclusion

We proposed a fast response and scattering free OILC phase comprised with thiol-ene and acrylate functional group monomers. The scattering was completely suppressed by matching the refractive index of the LC and polymer, and decreasing the LC droplet size below the visible wavelength range, resulting in an excellent dark state under crossed polarizer. The proposed PN393 device exhibits a higher transmittance (51%) and fast response time (40%) compared to conventional thiol-ene (NOA65) device reported elsewhere. The OILC with PN393 with optimized UV dosage is showing much less scattering than that of NOA65 although the amount of LC in PN393 is much higher than that of NOA65. The proposed device has a high potential to be applicable to flexible LCDs.

Funding

References

1. S. Matsumoto, M. Houlbert, T. Hayashi, and K. Kubodera, "Fine droplets of liquid crystals in a transparent polymer and their response to an electric field," Appl. Phys. Lett. **69**(8), 1044–1046 (1996).
2. S. Matsumoto, Y. Sugiyama, S. Sakata, and T. Hayashi, "Electro-optic effect, propagation loss, and switching speed in polymers containing nano-sized droplets of liquid crystal," Liq. Cryst. **27**(5), 649–655 (2000).
3. Y. Tanabe, H. Furue, and J. Hatano, "Optically isotropic liquid crystals with microsized domains," Mater. Sci. Eng. B **120**(1–3), 41–44 (2005).
4. S.-G. Kang and J.-H. Kim, "Optically-isotropic nanoencapsulated liquid crystal displays based on Kerr effect," Opt. Express **21**(13), 15719–15727 (2013).
5. S.-W. Choi, S.-I. Yamamoto, T. Iwata, and H. Kikushi, "Optically isotropic liquid crystal composite incorporating in-plane electric field geometry," J. Phys. D Appl. Phys. **42**(11), 112002 (2009).
6. S. Aya, K. V. Le, F. Araoka, K. Ishikawa, and H. Takezoe, "Nanosize-induced optically isotropic nematic phase," Jpn. J. Appl. Phys. **50**(5R), 051703 (2011).
7. R. Manda, S. Pagidi, M. Kim, C. H. Park, H. S. Yoo, K. Sandeep, Y. J. Lim, and S. H. Lee, "Effect of monomer concentration and functionality on electro-optical properties of polymer-stabilised optically isotropic liquid crystals," Liq. Cryst. **45**(5), 736–745 (2018).
8. W. Li, H. Cao, M. Kashima, F. Liu, Z. Cheng, Z. Yang, S. Zhu, and H. Yang, "Control of the microstrcucture of polymer network and effects of the microstructures on light scattering properties of UV-cured polymer-dispersed liquid crystal film," J. Polym. Sci., B, Polym. Phys. **46**(19), 2090–2099 (2008).
9. G. P. Montgomery, Jr., J. L. West, and W. Tamura-Lis, "Light scattering from polymer-dispersed liquid crystal films: Droplet size effects," J. Appl. Phys. **69**(3), 1605–1612 (1991).
10. J. Niziol, R. Weglowski, S. J. Klosowicz, A. Majchrowski, P. Rakus, A. Wojciechowski, I. V. Kityk, S. Tkaczyk, and E. Gondek, "Kerr modulators based on polymer-dispersed liquid crystal complexes," J. Mater. Sci. Mater. Electron. **21**(10), 1020–1023 (2010).
11. Y.-C. Yang and D.-K. Yang, "Electro-optic Kerr effect in polymer-stabilized isotropic liquid crystals," Appl. Phys. Lett. **98**(2), 023502 (2011).

12. J. H. Yu, H.-S. Chen, P.-J. Chen, K. H. Song, S. C. Noh, J. M. Lee, H. Ren, Y.-H. Lin, and S. H. Lee, "Electrically tunable microlens arrays based on polarization-independent optical phase of nano liquid crystal droplets dispersed in polymer matrix," Opt. Express **23**(13), 17337–17344 (2015).

13. M. J. Sansone, G. Khanarian, T. M. Leslie, M. Stiller, J. Altman, and P. Elizondo, "Large Kerr effects in transparent encapsulated liquid crystals," J. Appl. Phys. **67**(9), 4253–4259 (1990).

14. M. J. Sansone, G. Khanarian, and M. S. Kwiatek, "Large Kerr effects in transparent encapsulated liquid crystals. II. Frequency response," J. Appl. Phys. **75**(3), 1715–1721 (1994).

15. M. Torres-Cisneros, P. Likamwa, D. May-Arrioja, O. G. Ibarra-Manzano, H. Plascencia-Mara, E. Aguilera-Gómez, J. G. Aviña-Cervantes, J. J. Sanchez-Mondragon, Q. Song, J. A. Andrade-Lucio, and R. Guzmán-Cabrera, "Nano-droplet formation in polymer deispersed liquid crystals," Phys. Status Solidi. C. **9**(6), 1515–1520 (2012).

16. P. S. Drzaic, *Liquid Crystal Dispersions* (Singapore: World Scientific Publishing, 1995), Chap. 2.

17. S. J. Shin, N. H. Cho, Y. J. Lim, P. Nayek, S. H. Lee, S. H. Hong, H. J. Lee, and S. T. Shin, "Optically isotropic liquid crystal mixture showing high contrast ratio and fast response time," Proc. of the 11th International Meeting on Information Display (Society for Information Display, Seoul, Korea), 139–140 (2011).

18. C. -M. Chang, Y. -H. Lin, V. Reshetnyak, C. H. Park, R. Manda, and S. H. Lee, "Origins of Kerr phase and orientational phase in polymer-dispersed liquid crystal," Proc. of the SPIE 10361, 21st Liquid Crystals (SPIE Organic Photonics + Electronics, California, United State), 103610K (2017).

19. C. M. Chang, Y. H. Lin, V. Reshetnyak, C. H. Park, R. Manda, and S. H. Lee, "Origins of Kerr phase and orientational phase in polymer-dispersed liquid crystals," Opt. Express **25**(17), 19807–19821 (2017).

20. J. H. Yu, J. J. Lim, Y. J. Lim, P. Nayek, S. Kundu, S. W. Kang, and S. H. Lee, "Optically isotropic polymer dispersed liquid crystal composite for high contrast ratio and fast response time," SID Symposium Digest of Technical Papers **44**, 1338–1340 (2013).

21. N. H. Park, S. C. Noh, P. Nayek, M.-H. Lee, M. S. Kim, L.-C. Chien, J. H. Lee, B. K. Kim, and S. H. Lee, "Optically isotropic liquid crystal mixtures and their application to high-performance liquid crystal devices," Liq. Cryst. **42**(4), 530–536 (2015).

22. N. H. Cho, P. Nayek, J. J. Lee, Y. J. Lim, J. H. Lee, S. H. Lee, H. S. Park, H. J. Lee, and H. S. Kim, "High-Performance, in-plane switching liquid crystal device utilizing an optically isotropic liquid crystal blend of nanostructured liquid crystal droplets in a polymer matrix," Mater. Lett. **153**, 136–139 (2015).

23. V. K. Baliyan, S. H. Lee, and S.-W. Kang, "Optically and spatially templated polymer architectures formed by photopolymerization of reactive mesogens in periodically deformed liquid crystals," NPG Asia Mater. **9**(8), e429 (2017).

24. R. J. D. Tilley, *Color and the Optical Properties of Materials* (Willey: John Wiley & Sons, Ltd, 2011), Chap. 2.

25. J. Yan, L. Rao, M. Jiao, Y. Li, H.-C. Cheng, and S.-T. Wu, "Polymer-stabilized optically isotropic liquid crystals for next-generation display and photonics applications," J. Mater. Chem. **21**(22), 7870–7877 (2011).